Merging of range images for inspection or safety applications

James Mure-Dubois and Heinz Hügli

University of Neuchâtel - Institute of Microtechnology, 2000 Neuchâtel, Switzerland

ABSTRACT

Range imagers provide useful information for part inspection, robot control, or human safety applications in industrial environments. However, some applications may require more information than range data from a single viewpoint. Therefore, multiple range images must be combined to create a three-dimensional representation of the scene. Although simple in its principle, this operation is not straightforward to implement in industrial systems, since each range image is affected by noise. In this paper, we present two specific applications where merging of range images must be performed. We use the same processing pipeline for both applications : conversion from range image to point clouds, elimination of degrees of freedom between different clouds, validation of the merged results. Nevertheless, each step in this pipeline requires dedicated algorithms for our example applications. The first application is high resolution inspection of large parts, where many range images are acquired sequentially and merged in a post-processing step, allowing to create a virtual model of the part observed, typically larger than the instrument's field of view. The key requirement in this application is high accuracy for the merging of multiple point clouds. The second application discussed is human safety in a human/robot environment: range images are used to ensure that no human is present in the robot's zone of operation, and can trigger the robot's emergency shutdown when needed. In this case, range image merging is required to avoid uncertainties due to occlusions. The key requirement here is real-time operation, namely the merging operation should not introduce a significant latency in the data processing pipeline. For both application cases, the improvements brought by merging multiple range images are clearly illustrated.

Keywords: 3D vision, range imaging, sensor fusion, calibration, high resolution inspection, time of flight, RANSAC

1. INTRODUCTION

In recent years, usage of range sensors has increased, touching a wide variety of applications, going from city modeling[1] to cultural heritage[2], from safety systems[3] to inspection of small mechanical parts[4]. In many of those applications, a single measurement may fail to provide all the required information. To obtain a 3D model of a large part, multiple range images must be stitched together. Or, when occlusions occur, the uncertainty must be lifted through another measurement. In order to merge range images, the different data sets must be aligned. Alignment is performed by pairing data samples in both sets, either interactively, or automatically, such as in the *iterative closest point* (ICP)[5] approach. The choice of the appropriate alignment method will be constrained by the application considered, and depends on parameters such as camera configuration, geometry of the parts observed (for example, ICP fails on flat surfaces), and noise level. In this paper, we consider two range imaging systems employed in different applications. For each application, we describe the image acquisition configuration, explain the need for range data fusion, and propose an adequate alignment method for this fusion. The first system is a 3D microscope, used in an inspection application, where the part to inspect is imaged from top at a high resolution. In this case, the field of view is limited. Merging range images allows to create a larger, virtual 3D field of view. The second system considered is a network of real-time range cameras, used for a human safety application : the cameras acquire the same scene from different viewpoints, allowing to avoid occlusion problems found in monocular systems[3].

Section 2 describes the main properties of the two range imaging systems considered. Section 3 presents background knowledge for merging of range images, and introduces a random sample consensus (RANSAC) method to identify plane primitives. This method was applied on different data sets to validate the merging procedure, and in some cases to enable the merging. Experimental results are discussed in section 4. Finally section 5 provides a conclusion and insights about future developments of this work.

Table 1. Characteristics of 3D microscope system

Operation	Range map size	Field of view	Best case accuracy	Typical accuracy	Frame rate
Zoom 1×	997 × 1016	10 × 10 mm	50 μm	250 μm	0.02 fps
Zoom 10×	997 × 1016	1 × 1 mm	5 μm	25 μm	0.04 fps

Table 2. Characteristics of the SR-3000 camera

Operation	Range map size	Field of view	Best case accuracy	Typical accuracy	Frame rate
Close range	176 × 144	1 × 1 m	10 mm	50 mm	30 fps
Long range	176 × 144	5 × 5 m	50 mm	350 mm	20fps

2. CONSIDERED RANGE IMAGING SYSTEMS

This study is focused on two systems which can benefit of the improvements brought by range image merging. The first system is a 3D microscope, used for example in industrial inspection applications, and is characterized by a small field of view. The second system is a network of real-time range cameras. Such a network can be used in human safety applications, and must comply with stringent timing requirements. In the next paragraphs, we describe the measurement principle of those two systems, along with their main characteristics.

2.1 3D microscope

This system is a motorized microscope with a custom depth from focus software, allowing to produce range maps of objects smaller than 10 mm. The depth from focus principle is described by Zamofing *et al.*[4], and will only be summarized briefly here. In order to produce a range map, a series of images are grabbed while the microscope is moved vertically above the sample. The local sharpness is analyzed in each image. For each pixel in the final range image, the depth is computed as the maximum of local sharpness.

The Leica MZ12 microscope used in this setup has a variable zoom (1× to 10×). A Märzhäuser Control 2000 controller provides software interfaces to control the motion of an xy-platform for the sample and the z motion of the microscope body. The sensor used is a Pulnix Tm 1001 megapixel camera. The software used provides post-processing functions to enhance the quality of the final range map. Typical post-processing steps include multi-resolution filtering[6] and median filtering for noise removal. The main characteristics of this system are summarized in table 1. This system is well suited for the inspection of micro-mechanical parts with dimensions between 200 μm up to 10 mm. In the present paper, we will show that point cloud merging techniques allow to overcome this upper limit.

2.2 Time of flight camera network

The second system we consider is a network of real-time range imaging cameras based on the *time of flight* (TOF) measurement principle. Each camera actively emits a time varying infrared light signal, which is reflected by objects in the scene. The sensor pixels in the camera are able to reconstruct the signal from the reflected light, and therefore allow to measure the time elapsed for the light traveling back and forth from the camera. This *time of flight* map can then directly be converted into a range map, relative to the camera position. In the network, cameras are operated from different viewpoints. The viewpoints are not known *a-priori*, but adjusted in order to get the most complete representation of the scene (fig. 2). The alignment procedure should be able to merge data coming from devices for which the fields of view overlap partially.

The SwissRanger[7] SR-3000 and SR-3100 cameras used in our experiment are USB devices, capable of delivering up to 30 frames per second (*fps*). The main characteristics of those cameras are summarized in table 2. The viewing angle for the camera is roughly 45°, and the focal length is fixed ($f = 8\,mm$). Unfortunately, the sensor size is currently relatively small (176 × 144), but next generations of time of flight cameras should have improved resolution. Nevertheless, this type of range imager is particularly well suited to applications requiring to detect the position or motion of humans indoors, i.e. safety or human interface systems. We will illustrate below that merging multiple TOF range maps is beneficial in such applications.

(**a**) 3D microscope range map - Caliper part   (**b**) SwissRanger range map - Indoor scene

Figure 1. Range maps samples. The depth is intensity coded (**a**) or color coded (**b**).

3. MERGING OF RANGE IMAGES

The processing pipeline used to merge range images consists in first converting each range image to a point cloud, and then to merge those clouds in the same coordinates system. The next paragraphs describe how these tasks are performed for our two target systems. Finally, the success of the merge operation must be confirmed. Section 3.3 introduces geometric primitives used to confirm or enhance the quality of the merged results.

3.1 From range map to point clouds

The systems introduced in the previous section both produce range maps. A range map is defined as a 2D image where the pixel values encode the range to the object. Figure 1 shows sample ranges maps produced by 3D microscope and time of flight camera systems. Range maps can be converted to point clouds when the geometry of the projection onto the image plane is known. Each pixel in the range map defines one point of the cloud. In the following of the paper, we consider only point clouds and not meshes. Generally, a range map contains more information than a point cloud, since the 2D connectivity of the map can be used to define a meshing of the cloud. However, this implicit meshing has disadvantages. First, implicit meshing creates bad polygons along edges. Moreover, when multiple range images overlap, the implicit meshes produced from each range map exhibit many intersecting faces, since the noise is different in each mesh. Therefore, we report here only on fusion of point clouds. Investigation on fusion of meshes generated from range images is currently in progress.

3.1.1 3D microscope

For the 3D microscope range map, we make the assumption that the projection within the microscope field of view is *parallel*. Therefore considering the range map $R(i,j)$ of size $M \times N$, acquired with magnification setting m and z-scan intervals Δz, we can define the point cloud $\mathbf{P}$ such that :

$$\mathbf{P} = \{p_0, p_1, \ldots, p_L\} \qquad p_k = \begin{pmatrix} x \\ y \\ z \end{pmatrix} = \begin{pmatrix} x_0 + i \cdot m \cdot \Delta p_x \\ y_0 + j \cdot m \cdot \Delta p_y \\ z_0 + R(i,j) \cdot \Delta z \end{pmatrix} \qquad \begin{matrix} k = i \cdot N + j \\ \forall\, k = 0, 1, \ldots, L \\ L = (M \cdot N) - 1 \end{matrix} \qquad (1)$$

where $(\Delta p_x, \Delta p_x)$ is the sensor pixel pitch, (x_0, y_0) are the coordinates of the range image origin, and z_0 is the microscope altitude when acquiring the first image in the stack. (x_0, y_0, z_0) are with respect to the real-world origin, which can be set arbitrarily by the microscope user.

3.1.2 Time of flight camera

For this device, we use a *pinhole* camera model[8]. Knowing the camera focal length f and the position of the optical center (c_x, c_y) in pixel coordinates, along with the camera pixel pitch $(\Delta p_x, \Delta p_y)$, we can transform the range image $R(i,j)$ of size $M \times N$ into the point cloud $\mathbf{P}$:

$$\mathbf{P} = \{p_0, p_1, \ldots, p_L\} \qquad p_k = \begin{pmatrix} x \\ y \\ z \end{pmatrix} = \begin{pmatrix} (i - c_x) \cdot \Delta p_x \cdot \frac{z}{f} \\ (j - c_y) \cdot \Delta p_y \cdot \frac{z}{f} \\ R(i,j) \cdot \frac{f}{\sqrt{f^2 + ((i-c_x) \cdot \Delta p_x)^2 + ((j-c_y) \cdot \Delta p_y)^2}} \end{pmatrix} \qquad \begin{matrix} k = i \cdot N + j \\ \forall\, k = 0, 1, \ldots, L \\ L = (M \cdot N) - 1 \end{matrix}$$

$$(2)$$

In this case, the origin for the point cloud is the optical center of the camera.

3.2 Merging of point clouds

Two point clouds $\mathbf{P_1}$ and $\mathbf{P_2}$ which overlap partially can be merged if they are expressed in the same coordinates system. When this condition is met, the merged point cloud $\mathbf{P_m}$ is simply expressed as the *union* of both point clouds.

$$\mathbf{P_m} = \mathbf{P_1} \cup \mathbf{P_2} \tag{3}$$

Frequently, $\mathbf{P_1}$ and $\mathbf{P_2}$ are expressed in different coordinate systems. It is therefore necessary to determine a coordinate system transformation and express for example the points from $\mathbf{P_2}$ in $\mathbf{P_1}$'s coordinate system. The most general coordinate system transformation can be described by 7 independent parameters : 1 scale parameter (s), 3 translation parameters (t_x, t_y, t_z) and 3 rotation parameters (for example: r_x, r_y, r_z). If all those parameters are known, the transformation between coordinates system is simply expressed as a multiplication with a 4 transformation matrix $\mathscr{T}$.

$$\mathscr{T} = \begin{pmatrix} r_{11} & r_{12} & r_{13} & t_x \\ r_{21} & r_{22} & r_{23} & t_y \\ r_{31} & r_{32} & r_{33} & t_z \\ 0 & 0 & 0 & s \end{pmatrix} \qquad \mathbf{R} = \begin{pmatrix} r_{11} & r_{12} & r_{13} \\ r_{21} & r_{22} & r_{23} \\ r_{31} & r_{32} & r_{33} \end{pmatrix} = R_x \cdot R_y \cdot R_z \tag{4}$$

where R_x, R_y, R_z are represent 3D rotations around the elementary axes.

$$R_x = \begin{pmatrix} 1 & 0 & 0 \\ 0 & cos\,(r_x) & -sin\,(r_x) \\ 0 & sin\,(r_x) & cos\,(r_x) \end{pmatrix} \quad R_y = \begin{pmatrix} cos\,(r_y) & 0 & sin\,(r_y) \\ 0 & 1 & 0 \\ -sin\,(r_y) & 0 & cos\,(r_y) \end{pmatrix} \quad R_z = \begin{pmatrix} cos\,(r_z) & -sin\,(r_z) & 0 \\ sin\,(r_z) & cos\,(r_z) & 0 \\ 0 & 0 & 1 \end{pmatrix}$$

Most of the difficulty in the merging of range images then resides in the accurate determination of these 7 coefficients, in order to eliminate all degrees of freedom (DOF) in the expression of the transformation. The transformation itself is easily performed through multiplication with the quaternion $\mathscr{T}$. The amount of floating point multiplications required is $Mul_{fp} = 16 \cdot N_{cam} \cdot (M \cdot N)$, where N_{cam} is the number of cameras in the system, and $M \times N$ is the dimension of a camera frame. If the scales stay constant, only 9 multiplications per point are required, so that $Mul_{fp} = 9 \cdot N_{cam} \cdot (M \cdot N)$. For small point clouds such as those produced by TOF cameras, this computation can easily be performed in real-time.

3.3 Geometric primitives from point clouds

Although point clouds are sufficient for many applications of range imaging, it is sometimes desirable to group point with similar properties to achieve higher abstraction and robustness to noise. In particular, when range maps are obtained from scenes containing simple geometric shapes such as planes, cylinders, spheres or cubes, scene interpretation is facilitated when recognizing shapes as such rather than describing a long (and noisy) list of points lying on their surface[9]. In this paper, we consider and present an approach for the detection of planar patches based on the random sample consensus (RANSAC) method.

3.3.1 Planar patches by RANSAC

RANSAC is commonly used in the calibration of standard stereo systems[10]. We will briefly present its principle, and outline the specific usage of this method for the current study. The basic idea of RANSAC is simple : a (small) random set of measurements is used to parametrize a model $\mathscr{M}$. In our case, p points are selected randomly, and the least square plane defined by these points is computed. The least square plane is characterized by its normal vector $\vec{n}$ (our model). Then, the whole data set is compared to the model, and the fraction of measurements complying with the model is used as a score feature S. For a plane primitive, the distance to the plane is computed for all points in the cloud. If the distance is smaller than a fixed threshold d, the point is considered as *inlier* (belonging to the plane), and contributes to the score S for this model. The random selection and evaluation is repeated for a fixed number of iterations N. When this limit is reached, the model with the highest score S is then selected. When using appropriate values for d and N, it is possible to find the largest planar patch in the point cloud. The proper value for d will be directly related to the amount of noise present in the measurements.

Moreover, a new point cloud where all inliers have been removed can be defined. Applying the same RANSAC procedure on this point cloud allows to find the next largest planar patch. This process can be iterated as many times as necessary to identify all significant planar patches in the data set.

3.4 Plane primitives as quality check

The method described above can be used to check the quality of a point cloud $\mathbf{P_m}$ formed by the union of many point clouds $\mathbf{P_1}$ to $\mathbf{P_a}$ obtained from different range images $\mathbf{R_1}$ to $\mathbf{R_a}$. More specifically, the planar patches can be searched in each point cloud individually, or in the merged point cloud $\mathbf{P_m}$. Then, the results can be compared. If the merging operation is successful, all planar patches found in individual clouds must be found in the merged data. Moreover, planar patches corresponding to the same object in individual images should result in a single plane patch in the merged data.

3.5 Plane primitives as alignment help

As mentioned above, aligning point two clouds requires to determine 7 parameters, for the 7 DOF transformation between the two coordinates systems in which the clouds are defined. When point clouds are defined in absolute units, the scale parameter is easily obtained. Plane primitives can be used to obtain the remaining parameters. Each plane in 3D space can be defined by an equation of the form $ax + by + cz + d = 0$ where $\vec{n} = (a, b, c)^T$ is the normal to the plane. Pairing a single plane in both clouds allows to constrain the 3 rotation DOF. If another plane (not parallel to the first) can be paired in both clouds, only 1 DOF remains, corresponding to the translation along the line of intersection of the two planes. Finally, if three intersecting planes are paired, the coordinates transformation is fully determined. Section 4.1.2 provides an example of a practical aligment procedure involving one plane primitive.

4. APPLICATIONS

In this section, we provide examples based on real data sets. These examples illustrate how merging of point clouds can help to reach the goals we set for the microscope system and for the time of flight systems.

4.1 Imaging configurations

Our experiments involved two 3D measurement systems. We describe here the imaging configurations employed.

4.1.1 3D microscope : configuration

For the microscope inspection applications considered in this paper, we assume that the sample lies on an xy-platform, and that the microscope measures along the z axis. Therefore, the sample is always imaged from top, and there is no rotation between different point clouds acquired from the same sample. In this case, 4 degrees of freedom remain : translation (t_x, t_y, t_z) and scale s which can be varied by controlling the microscope zoom.

Since the motion of the sample and microscope are computer controlled during the 3D acquisition process, the translation parameters can simply be read and stored along with the range image. Provided that the zoom factor does not change between measurements, the coordinates transformation is then fully determined.

4.1.2 Multi TOF camera network : configuration

For the multi camera network, each TOF device is placed at a different position. The cameras are oriented so that the fields of view overlap partially (see fig. 2). Each device produces range maps relative to the center of its sensor. Neither the translations nor the rotations between different cameras are known *a-priori*. TOF cameras deliver absolute range values, so that the scale s will not vary between point clouds acquired with different cameras. Defining the coordinates system transformation between two point clouds produced with SwissRanger cameras therefore requires to determine 6 parameters, namely the translation (t_x, t_y, t_z) between the two sensor centers, and the rotation (r_x, r_y, r_z) between the two sensor planes.

While external measurements could provide an accurate estimation of the translation (t_x, t_y, t_z), the rotation (r_x, r_y, r_z) is difficult to measure *a-priori*. In the following paragraph, we describe a practical calibration method allowing to precisely determine the rotation between two TOF point clouds, under the assumption that both cameras acquire images of the same plane object during the calibration procedure[11].
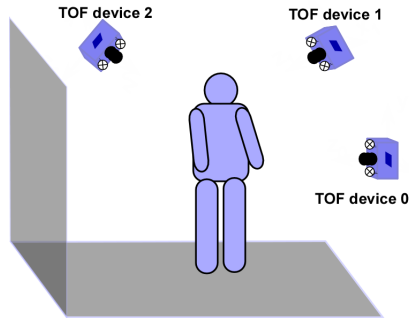
Figure 2. Schematic of a multi-camera network. All TOF cameras operate simultaneously. Each TOF device produces ranges images from a different viewpoint. The fields of view overlap partially.

Implemented alignment procedure   We employ RANSAC plane primitives in a practical alignment procedure for two TOF cameras. For this procedure, the cameras are pointed toward the same plane object, which must be the largest plane object in the cameras field of view. RANSAC is used to compute the normal $\vec{n}$ to this object in the coordinates system of each camera. Then, point clouds for each camera are rotated so that this normal becomes parallel to the z axis. Performing the rotation for both cameras ensures that calibration errors are evenly distributed between both clouds. When this step is completed, the remaining translation parameters are computed from a set of 6 to 10 point pairs defined by a human operator. Again, using more points helps in lowering the impact of measurement noise.

4.2 Field of view increase

In microscopy applications, the field of view is often limited. The merging procedure described above conveniently addresses this limitation. Our first example data set was produced from a part of caliper (Fig. **3a**). This sample is clearly larger than the microscope field of view (indicated by a red square). Therefore, four range map acquisitions were carried out sequentially, for partly overlapping fields of view. The resulting depth maps were then merged in a single point cloud, which allowed to produce a surface reconstruction of the sample. For this step, we used the surface reconstruction algorithm included in MeshLab[12]. Three renderings from different viewpoints of this reconstruction are shown in figures (Fig. **3b**) to (Fig. **3d**). This dataset clearly illustrates that field of view extension through point cloud merging produces accurate results.

This merging technique can be applied to real industrial parts, as illustrated in figure 4. In this example, a metallic part containing a hole was imaged. 5 range maps were acquired and combined. The system accuracy is sufficient to ensure a smooth surface reconstruction in the hole region, where as many as 4 range maps overlap. This example shows that the construction of virtual point clouds significantly larger than the microscope field of view is successful.

## 4.3 Quality check with plane primitives

As discussed in section 4.1.1, coordinates transformation for point clouds acquired with the 3D microscope setup can be directly stored during data acquisition. The following example illustrates that stitching such point clouds can be performed without compromising the extraction of plane primitives. Figure 5 shows a planar wooden part, from which 4 range maps were measured and combined. Points identified as belonging to the two largest planar regions are highlighted in cyan and yellow in figure **5c** and **5d**. In this experiment, where the field of view was $10 \times 10\,mm$, the threshold for plane inliers was set to $d = 50\,\mu m$. For each plane patch, 200 RANSAC iterations were performed. It appears clearly that points obtained from 4 different range maps with partial overlap are seamlessly merged in common plane patches.
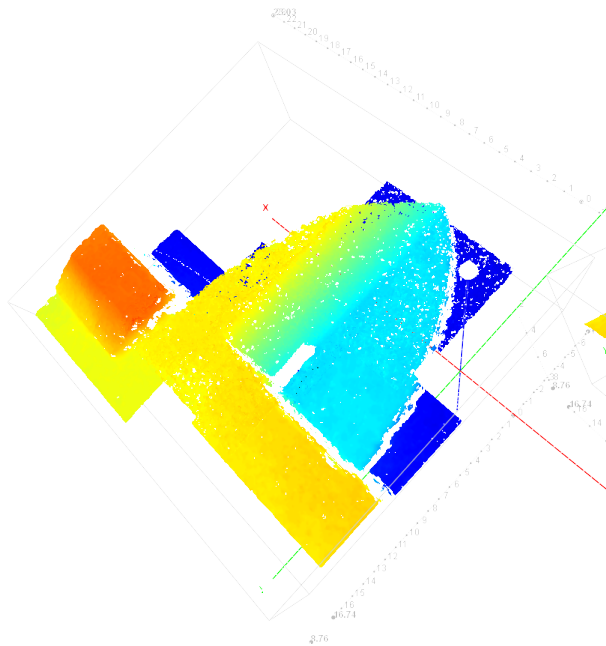
4.4 Alignment aided by plane primitives

Unlike in the microscope system, alignment is non-trivial in a TOF camera network. Therefore, we used the alignment procedure proposed in section 4.1.2. For the RANSAC procedure, the number of iterations N was
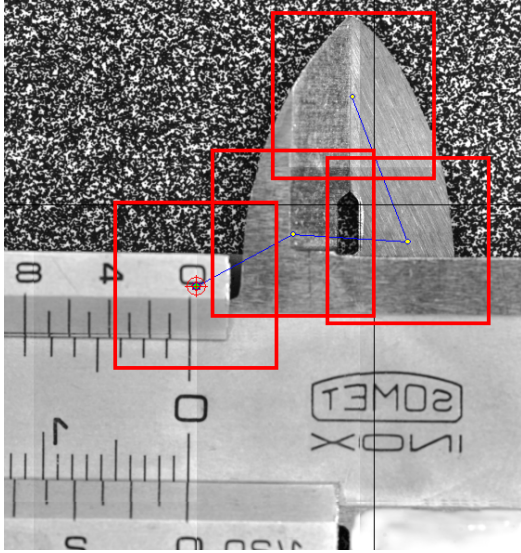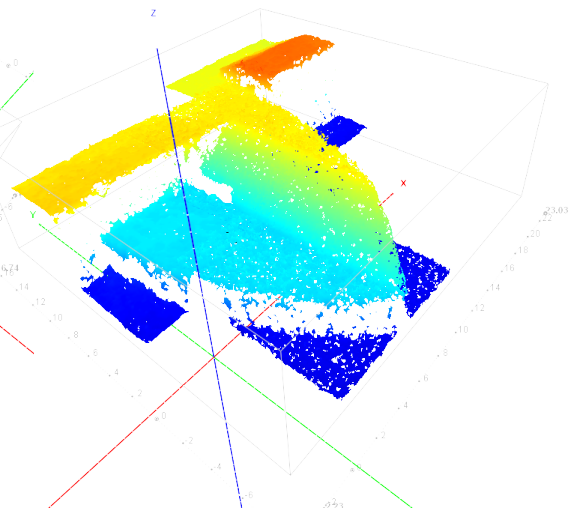
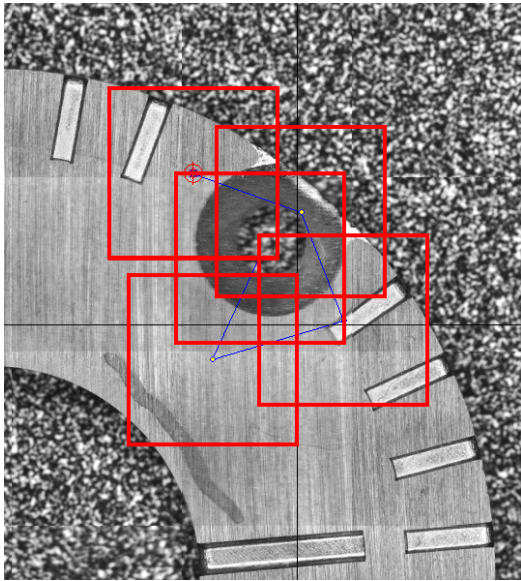(**a**) Intensity image of caliper. The microscope field of view is indicated by a red square.
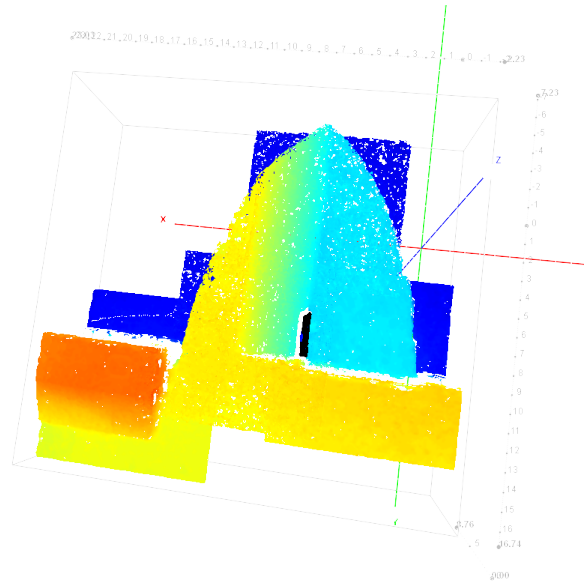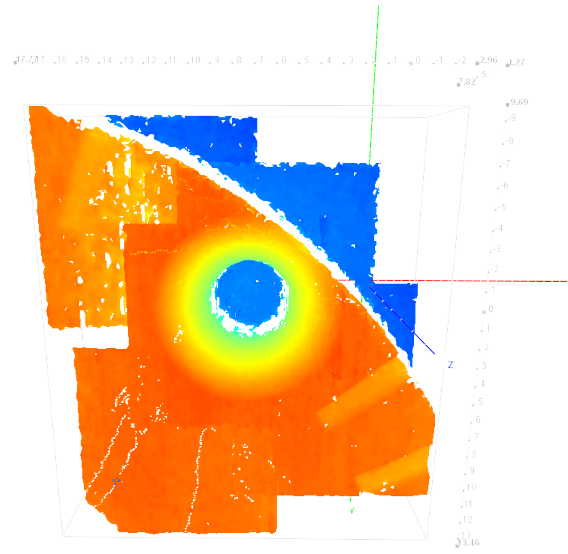
(**b**) View 1

(**c**) View 2

(**d**) View 3

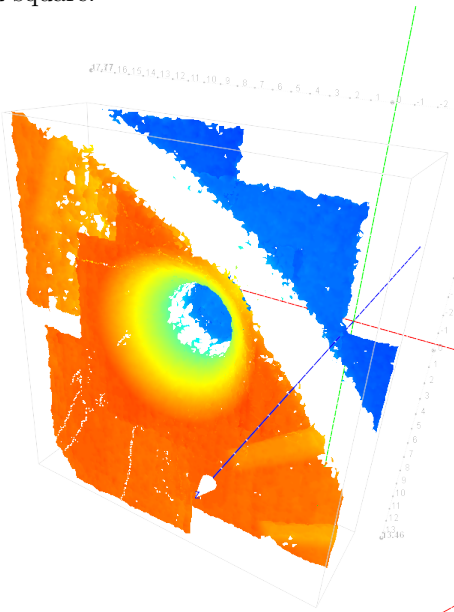Figure 3. Caliper with its 4 measured regions (**a**) and 3D display of merged range data (**b**, **c**, **d**)
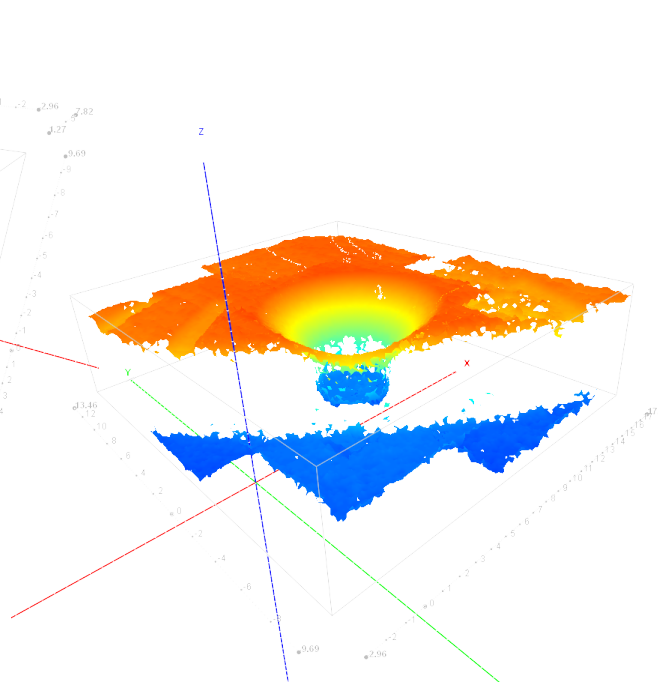
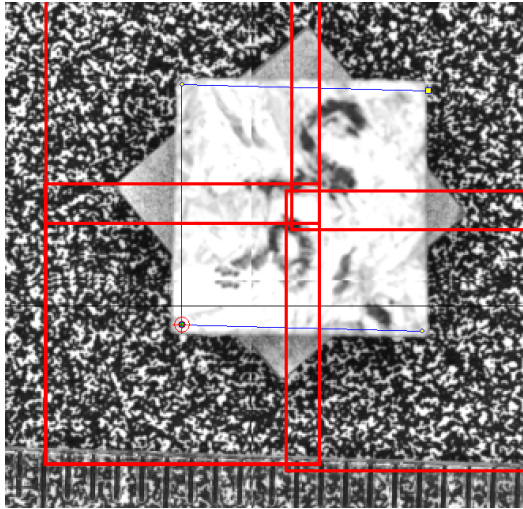(**a**) Intensity image of industrial part. The microscope field of view is indicated by a red square.
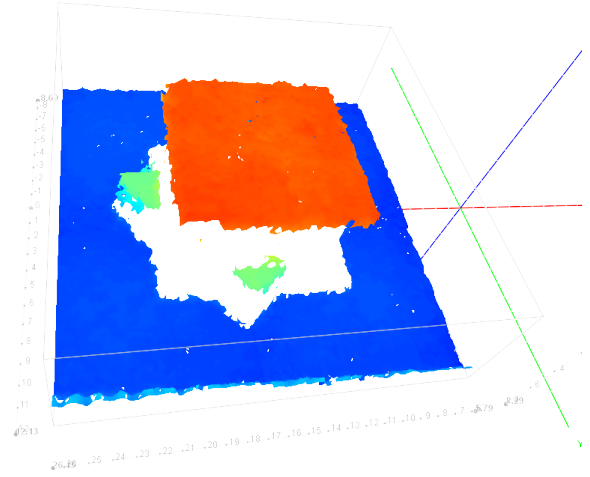

(**b**) View 1

(**c**) View 2

(**d**) View 3

Figure 4. Industrial part (with hole) with its 5 measured regions (**a**) and 3D display of merged range data (**b**, **c**, **d**)

(**a**) Intensity image of wooden. The microscope field of view is indicated by a red square.

(**b**) View 1
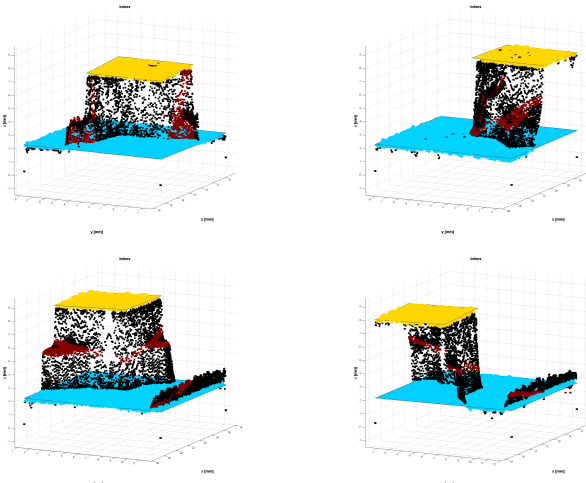
(**c**) Planar primitives in separate range images
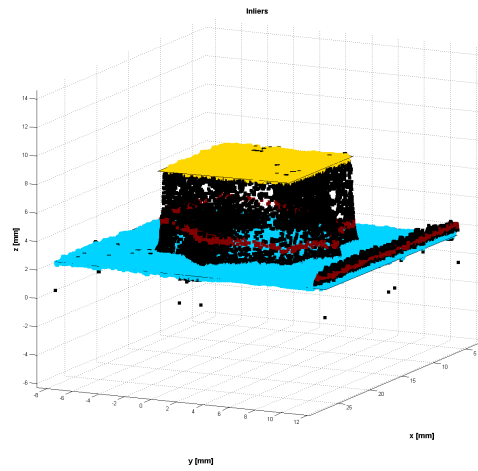
(**d**) Planar primitives for merged range data

Figure 5. Wooden part with its 4 measured regions (**a**) and 3D display of merged range data (**b**). Points identified as belonging to the two largest planar regions are highlighted in cyan and yellow in **c** and **d** (Disregard dark red , which corresponds to the next plane candidate).
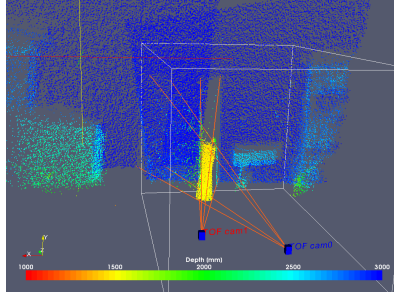
(**a**) Empty scene - Color image
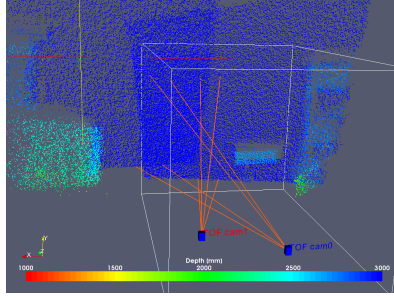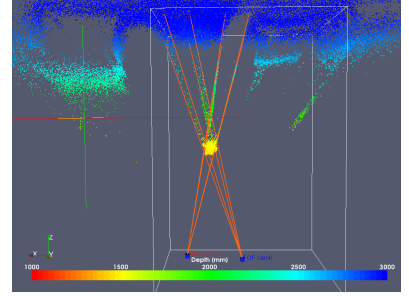
(**b**) Empty scene - Point cloud perspective view
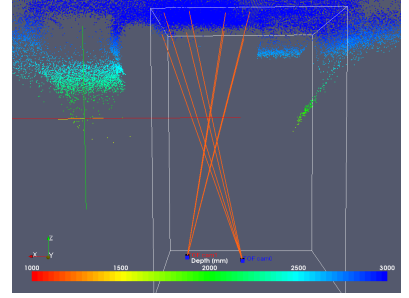
(**c**) Empty scene - Point cloud top view

(**d**) Scene with object - Color image

(**e**) Scene with object - Point cloud perspective view

(**f**) Scene with object - Point cloud top view

Figure 6. Test scene for occlusion removal. - The cardbox materializes a safety zone. Projection of the safety zone onto each camera sensor is displayed with orange lines in the point cloud representation.

set to 1600 and the threshold for inliers was $d = 350\,mm$. Although this threshold is quite large, the obtained rotation parameters do not suffer greatly from noise, since the plane orientation is determined by averaging on a sufficiently large number of inliers. Typically, good results are obtained when the number of inliers exceeds 10000. The remaining translation degrees of freedom were handled by manually defining 10 point pairs in the amplitude images provided by the Swissranger cameras. Section 4.5, which describes occlusion removal, provides a practical example of a dataset where point clouds from two Swissranger cameras where merged using this alignment method (see fig. 7).
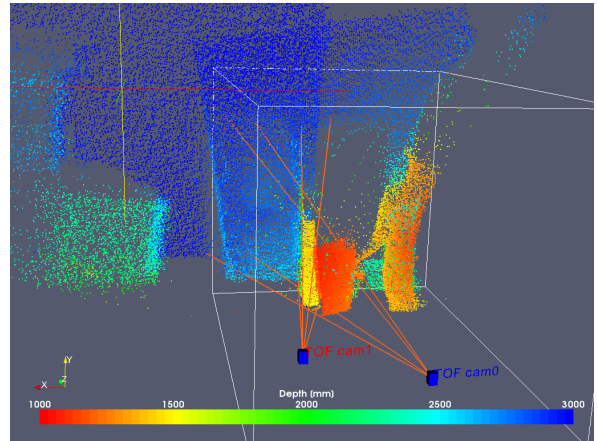
4.5 Occlusion removal

Kohoutek[3] proposes to use a time of flight camera in safety systems where humans and robots share the same workspace. However, a single viewpoint range imaging system, such as the SwissRanger SR-3100 may not be sufficient when occlusions occur. The following experiment shows how the addition of a second range imager can help in circumventing occlusions. Figure 6 shows an example indoor scene. In the bottom row images, a cardbox materializes a safety zone. Any human entering this zone should trigger the system emergency shutdown. Figure 6b,c,e,f shows different views of the merged point cloud obtained from range images shot with two SR cameras. In those images, the projection of the safety zone onto each camera sensor is materialized by orange lines. When each camera is operated individually, an alarm must be sent sent for each situation where an object enters the zone delimited by these lines. In figure 7, another object occludes the safety zone for rightmost camera (see fig. 7a,d). This situation would result in a false alarm.

When combining both cameras, the occlusion is circumvented. The safety zone is formed by the *intersection* of the projections for each camera. For this system this system, the coordinate transformation requires less than 500k floating point multiplications. This overhead does not bring a significant penalty in real-time applications, and can therefore be used in safety systems. Only the alignment procedure (using RANSAC) must be performed offline. We must note that using multiple cameras can also be used to increase the field of view : the merged point cloud in fig. 7 describes a larger scene than what could be obtained with a single SwissRanger.
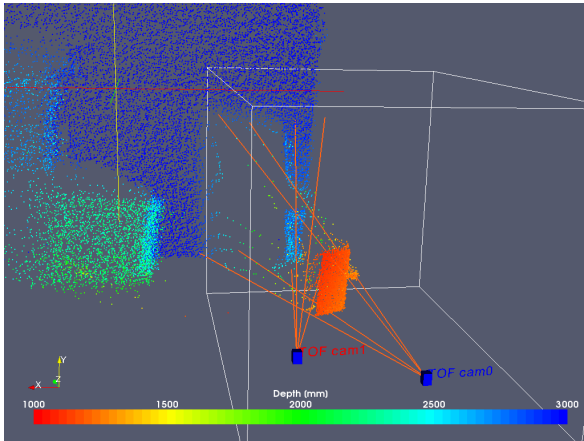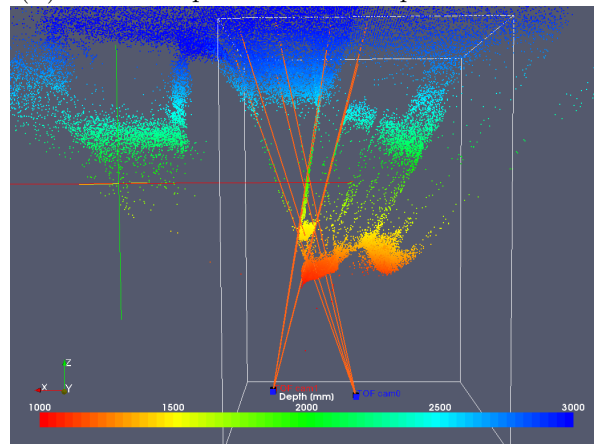
(**a**) Left point cloud - Perspective view

(**b**) Combined point cloud - Perspective view
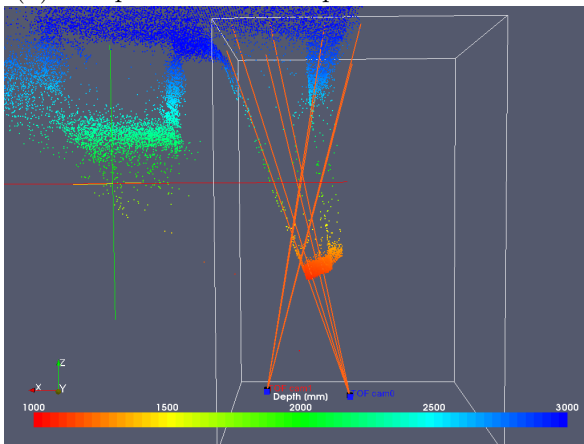
(**c**) Left point cloud - Top view

(**d**) Combined point cloud - Top view

Figure 7. Occlusion removal - Target cardbox is occluded in left point cloud (**a**, **c**). Using two cameras allows to remove occlusion (**b**, **d**).

5. CONCLUSION

In this paper we discussed the merging of multiple range images, for two systems used in different domains : a 3D microscope and a network of TOF cameras. We presented the main characteristics of those two systems, and described in each case how the range data is transformed into point clouds. The merging procedure requires to precisely align different points clouds. We considered geometric primitives extraction from point clouds, and illustrated how such primitives can be used to check the quality of the aligned result, or to help in the alignment process. For our first application, 3D microscopy, we observed that alignment is simple since no rotation is involved. Range image stitching allows to lift the constraint of limited field of view, opening the way to detailed inspection of large three dimensional parts. We provided examples of point clouds assembling up to 5 sequentially acquired microscope range maps. Plane primitives obtained through RANSAC allowed to validate the quality of the merged point cloud results.

For TOF camera networks, the alignment procedure requires to determine both rotation and translation parameters for each device pair in the network. In this case, using plane primitives obtained through RANSAC enhances the alignment quality. This alignment allows to virtually extend the field of view in scenes imaged in real-time by multiple cameras. Moreover, when single viewpoints systems are penalized by occlusion phenomena, the penalty is reduced for multi camera setups. We illustrated how robustness to occlusion can help reduce the number of false alarms in human safety systems.

We also mentioned some options to extend the present work to more demanding applications. Employing RANSAC methods to identify geometric primitives in point clouds enables creating automated part inspection systems. Moreover the connectivity information present in range maps could be used to create 3D meshes rather than point clouds. In this case, suitable filters must be developed to control problems at edges, or problems due to noise, in order to successfully merge the meshes.

REFERENCES

[1] Tarsha-Kurdiand T. Landes, F. and Grussenmeyer, P., "Hough-transform and extended ransac algorithms for automatic detection of 3d building roof planes from lidar data," in [*ISPRS Proceedings. Workshop Laser scanning. Espoo, Finland*], (2007).

[2] Weyrich, T., Pauly, M., Keiser, R., Heinzle, S., Scandella, S., and Gross, M., "Post-processing of scanned 3d surface data," in [*Proc. of Eurographics Symposium on Point-Based Graphics 2004*], 85–94 (2004).

[3] Kohoutek, T., "Monitoring of an industrial robot by processing of 3d-range-imaging data measured by the swissranger® sr-3000," in [*Proc. of Optical 3-D Measurement Techniques VIII, Zurich, Switzerland*], (2007).

[4] T. Zamofing and H. Hügli, "Applied multifocus 3D microscopy," in [*Two- and Three-Dimensional Vision Systems for Inspection, Control, and Metrology.*], Batchelor, B. G. and Hügli, H., eds., *Proc. SPIE* **5265**, 134–144 (2004).

[5] Jost, T. and Hügli, H., "A Multi-Resolution ICP with Heuristic Closest Point Search for Fast and Robust 3D Registration of Range Images," in [*Proc. 3Dim2003, 4th Int. Conf. on 3-D Digital Imaging and Modeling*], **PR01991**, 427–433 (Oct. 2004).

[6] T. Zamofing and H. Hügli, "Multiresolution reliability scheme for range image filtering," in [*Two- and Three-Dimensional Vision Systems for Inspection, Control, and Metrology II.*], Harding, K. G., ed., *Proc. SPIE* **5606**, 98–105 (2004).

[7] Mesa Imaging, "Swissranger SR-3000," (2007). http://www.mesa-imaging.ch/prodviews.php.

[8] Kahlmann, T., *Range imaging metrology : investigation, calibration and development*, PhD thesis, Eidgenössische Technische Hochschule ETH Zürich (2007).

[9] Schnabel, R., Wessel, R., Wahl, R., and Klein, R., "Shape recognition in 3d point-clouds," in [*Proc. of The 16-th International Conference in Central Europe on Computer Graphics, Visualization and Computer Vision'2008*], Skala, V., ed. (2008).

[10] Torr, P. and Murray, D., "The development and comparison of robust methods for estimating the fundamental matrix," *International Journal of Computer Vision* **24**, 271–300 (1997).

[11] Mure-Dubois, J. and Hügli, H., "Fusion of time of flight camera point clouds," (2008). submitted.

[12] Visual Computing Lab ISTI - CNR, "MeshLab v1.1.1," (2008). Tool developed with the support of the Epoch NOE - URL http://meshlab.sourceforge.net/.